Title	Transitions in the quantum computational power
Author(s)	Wei, Tzu-Chieh; Li, Ying; Kwek, Leong Chuan
Citation	Wei, T.-C., Li, Y., & Kwek, L. C. (2014). Transitions in the quantum computational power. Physical Review A, 89(5), 052315-.
Date	2014
URL	http://hdl.handle.net/10220/19763
Rights	© 2014 American Physical Society. This paper was published in Physical Review A and is made available as an electronic reprint (preprint) with permission of American Physical Society. The paper can be found at the following official DOI: http://dx.doi.org/10.1103/PhysRevA.89.052315. One print or electronic copy may be made for personal use only. Systematic or multiple reproduction, distribution to multiple locations via electronic or other means, duplication of any material in this paper for a fee or for commercial purposes, or modification of the content of the paper is prohibited and is subject to penalties under law.

Transitions in the quantum computational power

Tzu-Chieh Wei

*C. N. Yang Institute for Theoretical Physics and the Department of Physics and Astronomy, State University of New York at Stony Brook,
Stony Brook, New York 11794-3840, USA*

Ying Li

*Centre for Quantum Technologies, National University of Singapore, 2 Science Drive 3, Singapore and Department of Materials,
University of Oxford, Parks Road, Oxford OX1 3PH, United Kingdom*

Leong Chuan Kwek

*Centre for Quantum Technologies, National University of Singapore, 2 Science Drive 3, Singapore and National Institute of Education and
Institute of Advanced Studies, Nanyang Technological University, 1 Nanyang Walk, Singapore*

We construct two spin models on lattices (both two and three dimensional) to study the capability of quantum computational power as a function of temperature and the system parameter. There exists a finite region in the phase diagram such that the thermal equilibrium states are capable of providing a universal fault-tolerant resource for measurement-based quantum computation. Moreover, in such a region the thermal resource states on the three-dimensional lattices can enable topological protection for quantum computation. The two models behave similarly in terms of quantum computational power. However, they have different properties in terms of the usual phase transitions. The first model has a first-order phase transition only at zero temperature whereas there is no transition at all in the second model. Interestingly, the transition in the quantum computational power does not coincide with the phase transition in the first model.

I. INTRODUCTION

Transitions in phases of matter, such as melting of ice and boiling of water, is common in everyday life [1]. They also occur in zero temperature, where properties of the system are governed, instead of thermal effect, by quantum-mechanical fluctuations [2]. Tremendous understanding has been gained on the transitions in phases of matter. Recently, ideas from quantum information and computation [3] give rise to new perspectives on examining phases of matter, such as topological phases and their classification [4]. Moreover, from the viewpoint of computational universality in measurement-based quantum computation (MBQC) [5–9], a few works have suggested that resource states can emerge from certain quantum phases of matter [10–15] and that the transition in the quantum computational capability results in a new notion of phase transitions [16–19].

Here, we construct two models to investigate their ground states and thermal states for providing universal quantum computational resource for MBQC. As we shall see both models exhibit similar "phase diagrams" in terms quantum computational power, in both two and three dimensions. The advantage of three dimensions offers the possibility of topological protection in carrying out quantum computation, even at higher temperatures than in two dimensions. The two models are natural extension of a symmetric model that we considered previously [20], and the asymmetric parameter introduced here can be used to study its effect on computational universality, as well as the possibility to tune the system through a quantum phase transition. They are exactly solvable, and thus also allow us to study and compare with the usual transitions in phases of matter. The first model has a first-order phase transition only at zero temperature and it does not

coincide with the transition in the quantum computational power. Moreover, even though there is no phase transition at any finite temperature, there is a region at finite temperature that supports universal quantum computation. The second model does not have a phase transition at zero temperature but has a transition in quantum computational power at both zero and finite temperatures.

The remaining of the paper is organized as follows. In Sec. II we introduce the two models, which are defined on any trivalent lattices either in two or three dimensions. We focus on the ground-state properties as well as the phase diagram at finite temperatures. In Sec. III we discuss zero-temperature quantum computational capability and show the existence of a range of the system parameter, where the ground state can provide a useful resource for universal MBQC. In Sec. IV we turn to the finite temperatures and consider the thermal effects on quantum computational universality. We use the techniques of fault-tolerance quantum computation (FTQC) to map out regions in the phase diagram where FTQC can still be carried out by using thermal states for the universal MBQC. The corresponding phase diagrams of quantum computational power are obtained for both models in both two and three dimensions. It is worth mentioning that the three-dimensional (3D) models provide topological protection and hence the transition temperature in QC power is higher than that in two dimensions. We make concluding remarks in Sec. V.

II. TWO MODEL HAMILTONIANS

We have previously constructed a model Hamiltonian whose thermal states can be used for universal MBQC even without turning off the Hamiltonian [20]. The idea is to take a small unit of a few spins, e.g., one spin-3/2 $\vec{S}_i$ at the
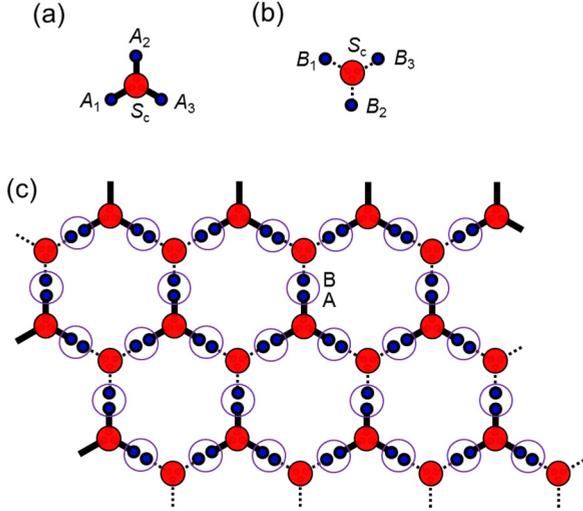
FIG. 1. (Color online) Illustration of bottom-up approach. Panels (a) and (b) illustrate the building block of one unit, which consists of one center spin-3/2 and three outer three virtual bond qubits. Two virtual bond qubits, each from a neighboring unit, form a physical bond spin-3/2 particle, as shown by circles enclosing them in (c). A two-dimensional or three-dimensional structure can be constructed.

center coupled to three outer spin-1/2 $\vec{s}_j$ that interact via the Heisenberg interaction $\vec{S}_i \cdot \vec{s}_j$; see Fig. 1. Then we stack up many such units to form a higher dimensional structure, e.g., the decorated 2D honeycomb or other trivalent lattices, or even 3D lattices, and then "glue" or map two smaller spins (i.e., spin-1/2 particles) from neighboring units to single larger spin; see, e.g., Fig. 1. Each merged spin, which we shall refer to as a bond particle, possesses a Hilbert space of dimension 4 (i.e., two copies of a qubit) and hence is equivalent to a spin-3/2 entity. One advantage of this approach is that the ground state and its spectral gap can be readily solved and checked. As we shall see, the exactly solvable Hamiltonians thereby constructed allow for fault-tolerant, universal quantum computation with thermal states, and even with topological protection in three dimensions [20].

There was no free parameter in the Hamiltonians in Ref. [20]. It was not clear whether or not such quantum computational universality only occurred for the specific Hamiltonian or could be extended to a region in a phase diagram. Here we use as building blocks two different types of interactions beyond the Heisenberg interaction to allow a free system parameter: the XXZ interaction $S_i^x s_j^x + S_i^y s_j^y + \Delta S_i^z s_j^z$ and an additional on-site anisotropic term $\vec{S}_i \cdot \vec{s}_j - d_z(S_i^z)^2$, and investigate relation between the statistical mechanical and quantum computational features of the resultant two- and three-dimensional models as the system parameter and the temperature vary. (Note that the upper case S_i is a spin operator for the center particle of larger spin magnitude, where s_j is a spin-1/2 operator, i.e., "half" of the degree of freedom in a bond particle and will be denoted by A or B later). These interactions might be engineered in cold atoms or trapped ions. It turns out to be useful to relate the ground-state wave functions of the two models if we parametrize Δ by

$\Delta = 1 + \delta$ in the first model and thus the Heisenberg point is at $\delta = d_z = 0$.

We thus arrive at two spin models. The Hamiltonian for model I consists of two types of interactions: $H_{\rm I} = \sum_{\rm line} V_{\rm line} + \sum_{\rm dash} V_{\rm dash}$, where

$$V_{\rm line} = S_c^x A_b^x + S_c^y A_b^y + (1+\delta)S_c^z A_b^z, \tag{1}$$

$$V_{\rm dash} = S_c^x B_b^x + S_c^y B_b^y + (1+\delta)S_c^z B_b^z, \tag{2}$$

where A_b^α's and B_b^β's are two independent spin-1/2 operators for the two virtual qubits of a bond particle. For model II, $H_{\rm II} = \sum_{\rm line} V_{\rm line} + \sum_{\rm dash} V_{\rm dash} + \sum_c V_c$,

$$V_{\rm line} = S_c^x A_b^x + S_c^y A_b^y + S_c^z A_b^z, \tag{3}$$

$$V_{\rm dash} = S_c^x B_b^x + S_c^y B_b^y + S_c^z B_b^z, \tag{4}$$

$$V_c = -d_z(S_c^z)^2, \tag{5}$$

the V_c is a local term on the center particles. These two models can be placed on two- and three-dimensional lattices; see, e.g., the hexagonal lattice in Fig. 1 and the 3D lattice in Fig. 3(c).

A. Model 1: XXZ interaction in a building block

Consider the XXZ interaction for each unit. The Hamiltonian within each unit can be exactly solved. For $\delta > -2$ the ground-state energy is $E_0(\delta) = (-9 - 5\delta - 2\sqrt{9+4\delta^2})/4$ (see Fig. 2) and the ground-state wave function for a unit (which is unique and gapped) is

$$|\Psi(\delta)\rangle = N_0(\delta)\Big[-(|3/2,-3/2\rangle - |-3/2,3/2\rangle) + \frac{-2\delta + \sqrt{9+4\delta^2}}{3}(|1/2,-1/2\rangle - |-1/2,1/2\rangle)\Big], \tag{6}$$

where $N_0(\delta)$ is a normalization constant such that the wave function is properly normalized, the symbol $|m_c, m_s\rangle$ denotes the joint state of the center spin-3/2 ($|m_c\rangle$) and three outer virtual spin-1/2 particles (collectively denoted by $|m_s\rangle$). The examples of the latter are $|m_s = 3/2\rangle = |\uparrow\uparrow\uparrow\rangle$ and $|m_s = 1/2\rangle = (|\uparrow\uparrow\downarrow\rangle + |\uparrow\downarrow\uparrow\rangle + |\downarrow\uparrow\uparrow\rangle)/\sqrt{3}$. The ground-state wave function for the whole 2D system is simply a product of $|\Psi(\delta)\rangle$ over all units (modulo appropriate merging).

For $\delta \gg 1$, $|\Psi(\delta)\rangle \sim |3/2,-3/2\rangle - |-3/2,3/2\rangle$, which is a four-spin Greenberger-Horne-Zeilinger (GHZ) state. Because of the merging of outer spin-1/2 particles across two units, such entanglement is useful for quantum computation, as explained in Refs. [5] and [21]. As δ approaches 0, it reduces to Heisenberg interaction within a unit and universal quantum computation can be done on such a two-dimensional structure [20].

For $\delta < -2$, the ground states are doubly degenerate: $|3/2,3/2\rangle = |\Uparrow\uparrow\uparrow\uparrow\rangle$ and $|-3/2,-3/2\rangle = |\Downarrow\downarrow\downarrow\downarrow\rangle$, each of which is ferromagnetic within the unit (where we have used $\Uparrow$ and $\Downarrow$ to denote the $|\pm 3/2\rangle$ of the center particle). The ground-state energy is $E_0 = 9(1+\delta)/4$. At a small but finite temperature T (smaller than the gap above the ground space),
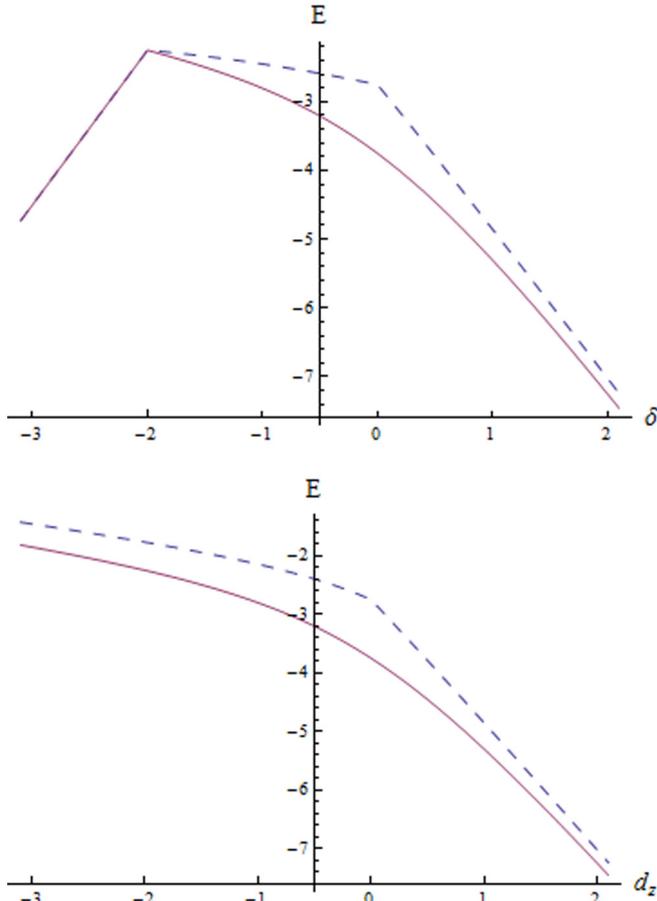
FIG. 2. (Color online) Ground-state and the first excited-state energies in each unit for the two models (top: model 1; bottom: model 2). The difference in the two energies is also the gap of the corresponding two- or three-dimensional models (for any finite system as well as in the thermodynamic limit). For the first model, the lowest two energy levels are degenerate for $\delta \leqslant -2$. The ground-state energy exhibits discontinuity in its first derivative with respect to δ, implying a first-order quantum phase transition in the model. However, for the second model, the ground-state energy is analytic for all range of d_z, implying nonexistence of phase transition.

the thermal state will be approximately $1/2|\Uparrow\uparrow\uparrow\uparrow\rangle\langle\Uparrow\uparrow\uparrow\uparrow| + 1/2|\Downarrow\downarrow\downarrow\downarrow\rangle\langle\Downarrow\downarrow\downarrow\downarrow|$, possessing no entanglement. Therefore, for $\delta < -2$, the whole system is not useful for universal quantum computation due to *lack* of entanglement.

The ground-state energy has discontinuity in its first-order derivative with respect to δ (see Fig. 2), i.e., there is a first-order phase transition. As the ground state in the ferromagnetlike phase, $\delta < -2$, cannot enable universal quantum computation, one is led to inquire whether universal quantum computation is possible for $\delta > -2$ and whether emergence of such computational power coincide with the phase transition.

B. Model 2: Heisenberg interaction with an on-site anisotropic term

In this section we consider interaction of the form $\vec{S}_i \cdot \vec{s}_j - d_z(S_i^z)^2$. As Pauli operators square to identity $\sigma_\mu^2 = \mathbb{1}$, there is no need to add a term $(s_i^z)^2$ for spin-1/2 particles. As it is

exactly solvable, the ground-state energy for a unit consisting of one center spin-3/2 and three outer spin-1/2 particles is $E_0(d_z) = (-9 - 5d_z - 2\sqrt{9 + 4d_z^2})/4$ for all range of d_z; see Fig. 2. Furthermore, the ground state (which is unique and gapped) is

$$
\begin{aligned}
|\Psi(d_z)\rangle = N_1(d_z)\Bigg[&-(|3/2,-3/2\rangle - |-3/2,3/2\rangle) \\
&+ \frac{-2d_z + \sqrt{9+4d_z^2}}{3}(|1/2,-1/2\rangle \\
&- |-1/2,1/2\rangle)\Bigg],
\end{aligned}
\tag{7}
$$

where $N_1(d_z)$ is a normalization constant such that the wave function is properly normalized. We see that the ground-state wave function and its energy are of the same form as in model 1 when $\delta > -2$. Hence, the computational power of the two models at zero temperature will be the same in the corresponding range. However, in contrast with model 1, this model does not have a phase transition in the state of matter. As this model contains the Heisenberg point, which is universal for MBQC, one is led to inquire whether the whole phase is universal (as there is no phase transition), as opposed to the first model.

III. CREATING A 2D CLUSTER STATE FROM GROUND STATES

We shall first consider the range of the parameters for the two models where ground state is of the same form within a unit:

$$
\begin{aligned}
|\Psi(a)\rangle \sim &-(|3/2,-3/2\rangle - |-3/2,3/2\rangle) \\
&+ \frac{1}{a}(|1/2,-1/2\rangle - |-1/2,1/2\rangle).
\end{aligned}
\tag{8}
$$

For model 1: the relation of a to δ (for $\delta > -2$) is given by

$$
a^{-1} = \frac{-2\delta + \sqrt{9+4\delta^2}}{3}.
\tag{9}
$$

For model 2: the relation of a to d_z (for all range of d_z) is given by

$$
a^{-1} = \frac{-2d_z + \sqrt{9+4d_z^2}}{3}.
\tag{10}
$$

Since the two models possess the same form of the ground-state wave function in the appropriate range of the parameters, we can deal with the quantum computational universality at zero temperature with equal footing. We note that, however, at finite temperatures the region of quantum computational universality will differ due to the different structures in the excited states and their energies. This will be treated in the next section.

The case $\delta = d_z = 0$ reduces to the Heisenberg interaction and the use for MBQC has been shown and detailed in Ref. [20] and this corresponds to $a = 1$. Examining the wave function (8), we see that we can recover the $a = 1$ wave function if we can apply the following operation on the center spin-3/2 particle:

$$
D(a) = \mathrm{diag}(1,a,a,1),
\tag{11}
$$

in the basis of $|3/2\rangle$, $|1/2\rangle$, $|-1/2\rangle$, and $|-3/2\rangle$. However, such a filtering operation cannot be realized with unit probability of success. This is because to implement a filtering operation such as $D(a)$, one needs to include another element $D'(a)$ to represent the unsuccessful filtering so that $D(a)^\dagger D(a) + D'(a)^\dagger D'(a) = \mathbb{1}$.

The solution is to use generalized measurement that can incorporate the filtering. For $a = 1$, the filtering is not needed and a generalized measurement has been used [20] so that a GHZ state, such as $(|3/2,-3/2\rangle - |-3/2,3/2\rangle)$, can be obtained within each unit. The POVM elements $\tilde{F}_\alpha$ (for spin-3/2's) were first constructed in Refs. [22,23],

$$\tilde{F}_x = \sqrt{\frac{2}{3}}(|3/2\rangle_x\langle 3/2| + |-3/2\rangle_x\langle -3/2|), \quad (12a)$$

$$\tilde{F}_y = \sqrt{\frac{2}{3}}(|3/2\rangle_y\langle 3/2| + |-3/2\rangle_y\langle -3/2|), \quad (12b)$$

$$\tilde{F}_z = \sqrt{\frac{2}{3}}(|3/2\rangle_z\langle 3/2| + |-3/2\rangle_z\langle -3/2|). \quad (12c)$$

For general a, we use a deformed POVM with elements $F_\alpha = q_\alpha(a)\tilde{F}_\alpha D(a)$ [$\alpha = x,y,z$ and the proportional constants $q_\alpha(a)$ are to be determined below] to act on the center particle so as to distill a GHZ state. The reason that $\tilde{F}_\alpha D(a)$ works can be illustrated by the example $\alpha = z$. First $D(a)$ restores the wave function back to the $a = 1$ case. Then $\tilde{F}_z$ filters out the GHZ state $(|3/2,-3/2\rangle - |-3/2,3/2\rangle)$, or equivalently, $|3/2\rangle|\downarrow\downarrow\downarrow\rangle - |-3/2\rangle|\uparrow\uparrow\uparrow\rangle$. If we choose to encode the effective qubit for the center particle by $|0\rangle \equiv -|-3/2\rangle$ and $|1\rangle \equiv |3/2\rangle$, and for the virtual spin-1/2's by the usual definition $|0\rangle \equiv |\uparrow\rangle$ and $|1\rangle \equiv |\downarrow\rangle$, then the resultant GHZ state for F_z outcome is

$$|\text{GHZ}\rangle = \frac{1}{\sqrt{2}}(|0000\rangle + |1111\rangle). \quad (13)$$

As the $a = 1$ wave function is symmetric under rotation, the case of $\alpha = x,y$ simply produces the GHZ state in the x and y bases, respectively. By imposing the completeness relation, $\sum_\alpha F_\alpha^\dagger F_\alpha = \mathbb{1}$, we find $q_x(a) = q_y(a) = 1/a$ and $q_z(a) = \sqrt{(3a^2 - 1)/(2a^2)}$. This can be verified easily by direction calculation that yields

$$F_x^\dagger F_x + F_y^\dagger F_y = \begin{pmatrix} \frac{1}{3a^2} & 0 & 0 & 0 \\ 0 & 1 & 0 & 0 \\ 0 & 0 & 1 & 0 \\ 0 & 0 & 0 & \frac{1}{3a^2} \end{pmatrix}, \quad (14)$$

$$F_z^\dagger F_z = \begin{pmatrix} 1 - \frac{1}{3a^2} & 0 & 0 & 0 \\ 0 & 0 & 0 & 0 \\ 0 & 0 & 0 & 0 \\ 0 & 0 & 0 & 1 - \frac{1}{3a^2} \end{pmatrix}. \quad (15)$$

In order for the above expressions to remain non-negative, such construction is valid only when $3a^2 \geqslant 1$. We note that a similar construction of positive operator-valued measure (POVM) has been first used in Ref. [19] in the context of a deformed Affleck-Kennedy-Lieb-Tasaki (AKLT) model. The POVM F_α's give rise to three possible outcomes, and any of them is a good

outcome. This effectively generates product of GHZ states among all units. However, the GHZ states are in different bases, depending on the outcome α. To fix the outcome basis in the z basis, we can imagine applying a unitary transformation to the post-POVM state if $\alpha = x$ or y. This is equivalent to using a different measurement basis for the effective qubits. For outcomes F_x and F_y, we perform operations U_y and U_x, respectively, where

$$U_y = \exp\left(i\frac{\pi}{2}\left(S_c^y + s_1^y + s_2^y + s_3^y\right)\right), \quad (16)$$

$$U_x = \exp\left(-i\frac{\pi}{2}\left(S_c^x + s_1^x + s_2^x + s_3^x\right)\right), \quad (17)$$

so that the resultant GHZ state is always of the form (13). Then measurement on the bond particle (i.e., a joint measurement on the two virtual qubits) can be used to induce a control-Z (CZ) gate between two center particles [20,24,25]. The result is a cluster state, a universal resource state. To summarize, we have thus shown that for $a \geqslant 1/\sqrt{3}$, the ground state is universal for MBQC.

For $a < 1/\sqrt{3}$, we need to use a different POVM [19], i.e.,

$$F_x' = \sqrt{3}\,\tilde{F}_x D(a), \quad F_y' = \sqrt{3}\,\tilde{F}_y D(a), \quad (18)$$

$$F_z' = \begin{pmatrix} 0 & 0 & 0 & 0 \\ 0 & \sqrt{1-3a^2} & 0 & 0 \\ 0 & 0 & \sqrt{1-3a^2} & 0 \\ 0 & 0 & 0 & 0 \end{pmatrix}. \quad (19)$$

One can easily verify the completeness relation $\sum_\alpha F_\alpha'^\dagger F_\alpha' = \mathbb{1}$, via a direct calculation that yields

$$F_x'^\dagger F_x' + F_y'^\dagger F_y' = \begin{pmatrix} 1 & 0 & 0 & 0 \\ 0 & 3a^2 & 0 & 0 \\ 0 & 0 & 3a^2 & 0 \\ 0 & 0 & 0 & 1 \end{pmatrix}, \quad (20)$$

$$F_z'^\dagger F_z' = \begin{pmatrix} 0 & 0 & 0 & 0 \\ 0 & 1-3a^2 & 0 & 0 \\ 0 & 0 & 1-3a^2 & 0 \\ 0 & 0 & 0 & 0 \end{pmatrix}. \quad (21)$$

In this case, the outcome F_z' is not desirable, i.e., it needs to be regarded as an error (specifically a qubit loss) as a GHZ cannot be obtained. The outcomes from F_x' and F_y' still yield a perfect GHZ state. To arrive at the same GHZ state (13) as in the case of $a \leqslant 1/\sqrt{3}$, we further perform operations U_y and U_x, for outcomes F_x' and F_y', respectively. Sites with undesirable outcome F_z' are equivalent to having leakage out of logical qubit space (or a qubit loss) but can be removed without affecting neighboring center sites by performing measurement on the surrounding bond particles so as to disentangle the unit (the center spin and the three virtual qubits) from the neighboring ones. Thus the qubit loss rate corresponds to the probability p_{delete} of obtaining a F_z' outcome, where

$$p_{\text{delete}} = \frac{1 - 3a^2}{1 + a^2}. \quad (22)$$

If $1 - p_{\text{delete}}$ is smaller than the site percolation threshold $p_{\text{th}}^{(\text{site})}$ (which depends on the lattices, such as honeycomb, cross, and square octagon), then there is not sufficient *connection* in the remaining network and thus no two-dimensional graph state can be distilled [17]. Fortunately, it turns out that there is a finite range of a below $1/\sqrt{3}$ such that the remaining sites still possess enough connection, i.e., the corresponding graph resides in the supercritical phase of percolation. For universal MBQC, it is thus required that $p_{\text{delete}} \leqslant 1 - p_{\text{th}}^{(\text{site})}$, i.e., $a^2 \geqslant p_{\text{th}}^{(\text{site})}/(4 - p_{\text{th}}^{(\text{site})})$. This gives $a^2 \gtrsim 0.211, 0.223, 0.229$ for honeycomb, square-octagon, and cross lattices, respectively. For the honeycomb lattice, the threshold translates to $\delta = d_z \gtrsim -1.2882$. Therefore, at zero temperature, there is a transition in the quantum computational power in both models and, in the first model, before the system reaches its phase transition at $\delta = -2$ as δ decreases. The exact location of the transition point in the quantum computational power depends on the underlying lattices, due to the connection to percolation. Connection to percolation and quantum computation has been previously explored, such as site percolation in noisy cluster states [17] and bond percolation in nondeterministic gates for cluster state preparation [26].

The above analysis shows that for model 1 the transition in the quantum computational power (at $\delta \approx -1.2882$ on the honeycomb lattice) does not coincide with the transition in the phase of matter (at $\delta = -2$). Moreover, even though model 2 possesses only one phase of matter, the quantum computational universality only exists in part of the phase. In

the following we shall investigate the finite-temperature effect on the quantum computational universality and determine the corresponding "phase diagram" in terms of quantum computational capability.

IV. THERMAL STATES AND FAULT TOLERANCE: TWO AND THREE DIMENSIONS

Because of the structure that the Hamiltonian for both models can be divided into units independent with one another, the free energy at finite temperatures are nonsingular, and thus there is no phase transition at finite temperatures. As we shall see below, the region with universal quantum computational power exists up to certain finite temperatures. For a finite temperature, the system is not in the exact ground state but a thermal state. This means that the production of a GHZ state in each unit (and thus the global cluster state) is faulty. Therefore, whether the "phase" of universal quantum computational power exists depends on how one can deal with errors. In particular, the phase boundary will depend on the error rates and the thresholds for fault-tolerant quantum

FIG. 4. (Color online) 2D Phase diagrams in terms of computational power: (a) Upper: the XXZ model; (b) bottom: the anisotropic model. In the region below the solid black curve the equilibrium thermal states provide universal resource for MBQC. For reference, the energies for the ground state and the first excited is shown in white curves (solid and dashed, respective).
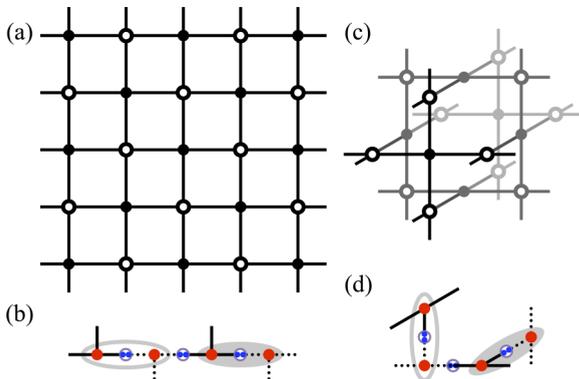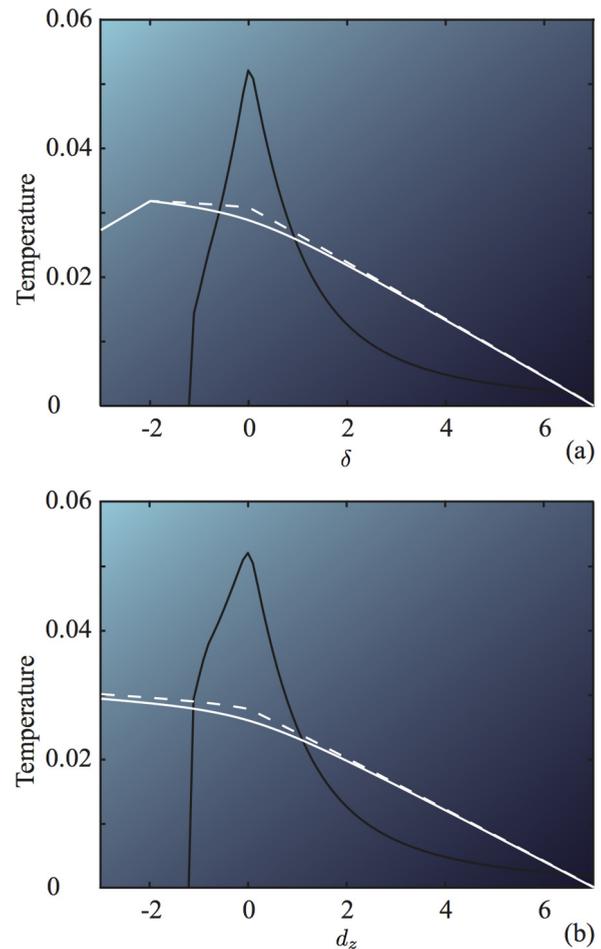
FIG. 3. (Color online) Lattices of cluster states and microscopic construction of qubits. Panel (a) is the 2D square-lattice cluster state, and (c) is the unit cell of the 3D bcc (body-center-cubic lattice) cluster state. Both could be constructed from trivalent lattices (with degree-3 nodes) using the modification as shown in (b) and (d), respectively, which converts a degree-4 node to combinations of degree-3 nodes; see also Ref. [27]. Note that with such a construction, (a) will be turned to a brick-wall structure equivalent to the honeycomb lattice shown in Fig. 1(c). See also Fig. 6 and the Appendix for the conversion. In (b) and (d), each logical qubit (oval) is composed of spins from two units. The spins inside each oval will eventually be converted to one logical qubit. The circle (which includes two virtual qubits, i.e., a single bond particle) between the two ovals is used to entangle neighboring two effective qubits (within the ovals) via measurement of a bond particle. Essentially, the product of two GHZ states from two such units can be converted to a single GHZ via local measurement on the bond particle inside the oval as well as one of the center particle.
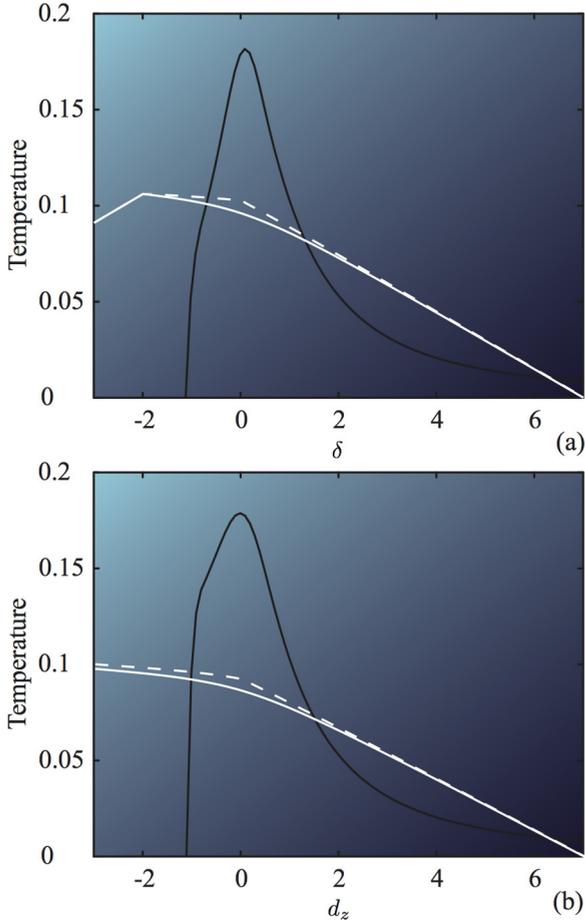
FIG. 5. (Color online) 3D phase diagrams in terms of computational power. (a) XXZ model; (b) anisotropic model. In the region below the solid black curve the equilibrium thermal states provide universal resource for MBQC. For reference, the energies for the ground state and the first excited is shown in white curves (solid and dashed, respective). Note that the transition temperatures are about three to four times higher than in two dimensions at the Heisenberg point.

computation (FTQC). Our goal is to establish the existence of a nonzero-temperature region that universal MBQC is possible rather than to pinpoint the absolute boundary of such a region. In the following we describe in detail the error analysis and how the "phase diagram" of the computational power is obtained. For those readers who wish to skip the details, the "microscopic" construction is in Fig. 3 and the resultant phase diagrams for both models are in Fig. 4 for two dimensions and in Fig. 5 for three dimensions.

For each set of particles, the thermal state reads

$$\rho_T = \frac{e^{-H/T}}{\mathrm{Tr}\, e^{-H/T}}, \qquad (23)$$

where H is the Hamiltonian of four spins including one spin-3/2 and three spin-1/2, and T is the temperature. As the input state is a thermal state, the output state after the POVM and the associated unitary operations is a noisy GHZ state. If $a > 1/\sqrt{3}$, the output state is

$$\rho_{\mathrm{GHZ}} = U_y F_x \rho_T F_x^\dagger U_y^\dagger + U_x F_y \rho_T F_y^\dagger U_x^\dagger + F_z \rho_T F_z^\dagger, \qquad (24)$$

and the success probability is $p_s = 1$. If $a < 1/\sqrt{3}$, the output state is

$$\rho_{\mathrm{GHZ}} = p_s^{-1}(U_y F_x' \rho_T F_x'^\dagger U_y^\dagger + U_x F_y' \rho_T F_y'^\dagger U_x^\dagger), \qquad (25)$$

where the success probability is $p_s = 1 - \mathrm{Tr} F_z' \rho_T F_z'^\dagger$, due to "loss" of logical quits.

The ideal GHZ state $|\mathrm{GHZ}\rangle$ (13) is the common eigenstate of the stabilizer elements $X_0 X_1 X_2 X_3$, $Z_0 Z_1$, $Z_0 Z_2$, and $Z_0 Z_3$ (this set is denoted by $\{K\}$) with the same eigenvalue $+1$. Here, X_0 and Z_0 are Pauli operators of the center qubit, and similarly for other three qubits. In order to use the fault-tolerant quantum computing (FTQC) theory to analyze the computational power, we convert imperfections in the noisy GHZ state ρ_{GHZ} into Pauli errors by randomly performing stabilizer operations, which results in

$$\rho_{\mathrm{GHZ}}' = \prod_{K \in \{K\}} \frac{1}{2}([\mathbb{1}] + [K])\rho_{\mathrm{GHZ}}, \qquad (26)$$

where $[\Lambda]\rho \equiv \Lambda \rho \Lambda^\dagger$. Here, $\{K\}$ is the set of the above stabilizer generators. Such randomization can be effectively performed by updating the basis of the ensuing single-particle measurements rather than actively by actively applying K's. The state ρ_{GHZ}' is thus diagonal in the basis of stabilizers and can be written as

$$\rho_{\mathrm{GHZ}}' = \sum_{\sigma \in \{\sigma\}} p_\sigma [\sigma] |\mathrm{GHZ}\rangle \langle \mathrm{GHZ}|, \qquad (27)$$

where $\{\sigma\}$ are Pauli operators listed in Table I, each $[\sigma]|\mathrm{GHZ}\rangle\langle\mathrm{GHZ}|$ corresponds to a common eigenstate of stabilizers, and $p_{\sigma \neq \mathbb{1}}$ is the probability of the corresponding Pauli error. If the eigenvalue of $X_0 X_1 X_2 X_3$ is -1 in an eigenstate, there is an error $[Z_0]$ in the state. Note that for convenience of notation we use X to denote the Pauli σ_x and Z the Pauli σ_z and one could also attribute -1 eigenvalue of $X_0 X_1 X_2 X_3$ to a $Z_{i=1,2,3}$ error instead of Z_0, but it is equivalent. Similarly, the -1 eigenvalue of $Z_0 Z_i$ corresponds

TABLE I. The Pauli operators $\{\sigma\}$ that appear in Eq. (27). X denotes Pauli σ_x and Z denotes Pauli σ_z. There are in total 15 different inequivalent errors that may occur on the noisy GHZ state. Subscript 0 denotes the center spin [i.e., c in Fig. 1(a)], and subscripts 1–3 denote the surrounding virtual qubits. The list only considers inequivalent errors; e.g., Z_0 and $Z_{i=1,2,3}$ errors produce the same consequence for the GHZ state (13), and hence either one of them, say, Z_0, is needed in Eq. (27) and listed in the table. Moreover, the triple X error $X_1 X_2 X_3$ is equivalent to a single X_0 error, i.e., $X_0 \equiv X_1 X_2 X_3$. The probabilities of these inequivalent errors for the example of the isotropic model, $\delta = d_z = 0$, are also listed at a temperature $T = 0.16$.

σ	Probability	σ	Probability
$\mathbb{1}$	0.9942	Z_0	3.45×10^{-3}
X_1	3.84×10^{-4}	$Z_0 X_1$	3.84×10^{-4}
X_2	3.84×10^{-4}	$Z_0 X_2$	3.84×10^{-4}
X_3	3.84×10^{-4}	$Z_0 X_3$	3.84×10^{-4}
$X_1 X_2$	2.38×10^{-9}	$Z_0 X_1 X_2$	2.38×10^{-9}
$X_2 X_3$	2.38×10^{-9}	$Z_0 X_2 X_3$	2.38×10^{-9}
$X_1 X_3$	2.38×10^{-9}	$Z_0 X_1 X_3$	2.38×10^{-9}
X_0	1.23×10^{-16}	$Z_0 X_0$	1.15×10^{-16}

TABLE II. Consequence of qubit errors (from 0-3 and 0'-3' of block C in Fig. 6) on logical cluster-state qubits. The logical error X_C is equivalent to $Z_U Z_L Z_D Z_R$ due to the cluster-state stabilizer operator $X_C Z_U Z_L Z_D Z_R$. Note that the Z_i's result in Z_C, and the probability of all such errors is already included in $2p_{Z_0}$.

Errors on 0-3 or 0'-3'	Errors on C, U, L, D, and R
X_0	I (no error)
$X_{0'}$	$X_C \equiv Z_U Z_L Z_D Z_R$
X_1 or $X_{1'}$	$Z_U Z_L$
X_2	Z_U
$X_{2'}$	Z_D
X_3	Z_L
$X_{3'}$	Z_R
Z_i (for all i)	Z_C

to an $[X_i]$ error. Therefore, error probabilities can be obtained from diagonal elements of ρ'_{GHZ}.

As seen above, in addition to single-qubit errors, some errors occur simultaneously, such as $[Z_0 X_i]$ and $[X_i X_j]$. In our numerical results, we find that only the $[Z_0 X_i]$ type of correlated errors are significant (see, e.g., Table I), and other correlated errors are negligible even at the transition point of the computation power, i.e., the FTQC threshold. Actually, these other correlated errors constitute less than 3% of the overall errors. Therefore, only the errors $[Z_0]$, $[X_i]$, and $[Z_0 X_i]$ will be taken into account in the following.

We can construct a 2D cluster state on the square lattice from the models sitting on the honeycomb lattice, as well as 3D cluster state from the models on the lattice proposed in Ref. [27], modified from a construction in Ref. [20] (see Fig. 3). In both cases, each qubit on the cluster state corresponds to two GHZ states. The procedure for obtaining a 2D cluster state on a square lattice is explained in detail in the Appendix, and is easily adapted to the 3D case. Moreover, the effect of errors on the cluster state can be analyzed straightforwardly, and is summarized in Table II. We describe them now. On the two GHZ states, each $[Z_0]$ error is propagated to a $[Z]$ error on the corresponding cluster-state qubit. We label the spin-$1/2$ bond particle measured for fusing two GHZ states as qubit 1. Then, each $[X_1]$ error is propagated to a correlated error $[ZZ]$ on two neighboring cluster-state qubits (see Table II). And, $[X_2]$ and $[X_3]$ errors are propagated to independent $[Z]$ errors on neighboring cluster-state qubits. Similarly, each $[Z_0 X_1]$ is propagated to a correlated error $[ZZZ]$ on the corresponding cluster-state qubit and two neighboring cluster-state qubits, and $[Z_0 X_2]$ and $[Z_0 X_3]$ errors are propagated to a correlated error $[ZZ]$ on the corresponding cluster-state qubit and one neighboring cluster-state qubit. Other types of errors on GHZ states have been neglected as they rarely occur. Therefore, on the final cluster state, the total probability of phase errors on each qubit is

$$p_z \simeq 2(p_{Z_0} + 2p_{X_1} + p_{X_2} + p_{X_3} \\ + 3p_{Z_0 X_1} + 2p_{Z_0 X_2} + 2p_{Z_0 X_3}), \qquad (28)$$

where p_{Z_0}, p_{X_i}, and $p_{Z_0 X_i}$ are probabilities of errors $[Z_0]$, $[X_i]$, and $[Z_0 X_i]$ on each GHZ state, respectively. The overall factor of 2 comes from the usage of two units to build one qubit in the cluster state. On the finial cluster state, there exist

(i) correlated errors $[ZZ]$ with a probability $2p_{X_1}$ on some pairs of qubits connected to the same qubit, (ii) correlated errors $[ZZ]$ with a probability $2p_{Z_0 X_2}$ or $2p_{Z_0 X_3}$ on each pair of directly connected qubits, and (iii) correlated errors $[ZZZ]$ with a probability $2p_{X_1}$ on some trimers formed by connected qubits. All the contribution of correlated errors to each single qubit has been included in p_z. Furthermore, because a cluster-state qubit is missing if one or two GHZ states are not successfully generated, the loss rate of cluster qubits is $p_l = 1 - p_s^2$.

The 2D cluster state on a square lattice can tolerate qubit loss up to a rate $\sim 40\%$ [17]. With a tolerable loss rate, a 2D graph-state network can be identified from the cluster state with qubit loss, which can be converted to a new 2D cluster state on a hexagonal lattice without qubit loss. The expected fraction of the new cluster state $k(p_l)$ [17], i.e., the average length of the path between nodes on the network is $1/k$, depends on the loss rate p_l (such a relation has been worked out numerically in Ref. [17]). The errors on each path may affect the two qubits, corresponding to the two connected nodes, on the final hexagonal lattice. Therefore, on the new cluster state, the probability of errors can be estimated as $p'_z \approx 3p_z/k$. Here the factor 3 is due to the three paths connected to each node on the network. The thresholds for FTQC on the 2D cluster state are more stringent than the thresholds for FTQC on one-dimensional circuit architectures by a factor of approximately 10^2 [28]. Because the one-dimensional-architecture thresholds (for the circuit model) are approximately 10^{-5} [29,30], we thus use 10^{-7} as the corresponding threshold of the 2D cluster-state model without qubit loss to estimate the phase boundary for the transition in quantum computational power. Therefore, the threshold of 2D models can be estimated as

$$p'_z \approx 10^{-7} \Rightarrow p_z \approx \tfrac{1}{3} 10^{-7} k(p_l). \qquad (29)$$

We numerically solve the temperature such that the above equation holds to determine the phase boundary. The resultant phase diagrams for both models are shown in Fig. 4.

On 3D cluster states, one can encode quantum information with topological codes, and hence error rates much higher than the 2D threshold are tolerable. Without qubit loss, the error rate threshold of 3D cluster states is 2.93% for independent phase-flip errors if the minimum-weight perfect matching algorithm is used to find the likely distribution of errors.

On the 3D cluster state obtained from the construction in Fig. 3(c), there are both independent errors and correlated errors. By choosing the arrangement of particles as shown in Fig. 3(d), the correlations occur between errors either on directly connected qubits or two qubits oppositely connected to the same qubit. The correlations of errors on directly connected qubits can be neglected due to the error correction algorithm, and the other type of correlations may affect the threshold but not significantly [31,32]. Numerical evidence suggests that the threshold decreases approximately linearly with the probability of qubit loss and it can be tolerated up to 24.9% [33]. As shown in [33], the threshold of 3D models can therefore be approximated as follows [33]:

$$\frac{p_l}{24.9\%} + \frac{p_z}{2.93\%} \approx 1. \qquad (30)$$

Below this critical line, errors are correctable and the resource state can be used for universal quantum computation. This

relation is then used to estimate the phase boundary for quantum computational power, as shown in Fig. 5.

V. CONCLUDING REMARKS

We have worked out the phase diagrams for the quantum computational power for two different models in both two and three dimensions. Our initial guess would be that such transition might coincide with that in phases of matter [19]. However, we find that instead quantum computational universality is more intricate and may not persist at all points of a certain phase of matter. The first model has a first-order phase transition at $\delta = -2$ at zero temperature but no phase transitions at nonzero temperatures. The isolated transition point does not locate at the boundary in the quantum computational power. Said equivalently, in this model the transition in the quantum computational power does not coincide with the transition in phases of matter. Such a noncoincidence was already hinted at in Ref. [19], where in the quantum computational universality is likely to disappear at certain point in the valence-bond solid phase. The second model does not have a phase transition at all but has a transition in quantum computational power at both zero and finite temperatures. The region with quantum computational capability for both models survives to higher temperatures in three dimensions than in two.

We also note that the ability to keep the interaction on while performing quantum computation is not a general feature of the model. It requires that all excited eigenenergies measured from the ground energy must be rational relative to one another [20]. This only occurs when $\delta = d_z = 0$, at which the models possess the highest symmetry. Incidentally, the closer to the symmetric point, the quantum computational power appears to sustain to a higher temperature. The only other model known to possess such a feature is actually the cluster-state model itself [7].

In our discussions of the FTQC thresholds, we have considered that the error sources come from the thermal effect, as we are interested in the computational-power phase diagram of the states themselves. By doing so we have assumed that measurements and other operations are perfect. These other errors can be included in the FTQC, and as long as their error rates are small enough, they can also be corrected by the error correction algorithm, but of course, will reduce the tolerable temperature.

APPENDIX: GENERATION OF CLUSTER STATES AND ERROR ANALYSIS

In this Appendix we describe how the merging and CZ gates are implemented by measuring bond particles. We also discuss the effect of errors on qubits. To simplify notation, we will omit the overall normalization. We assume that POVM's on all center particles have been carried out and these particles become effectively qubits. We illustrate how to obtain a cluster state on the square lattice, but it is easily adapted to the bcc lattice.

(I) First let us consider how to merge two GHZ states of the form $|0000\rangle + |1111\rangle$. This will be done by measuring the two virtual qubits that form a bond particle. Denote other qubits not involved by an underline, i.e., $|0000\rangle + |1111\rangle \rightarrow |\underline{00}\rangle + |\underline{11}\rangle$. The two virtual qubits will be measured in the basis $\{|00\rangle \pm |11\rangle, |01\rangle \pm |10\rangle\}$, i.e., a particular basis for the associated spin-3/2 bond particle. For example, an outcome of $|00\rangle + |11\rangle$ will project the two pairs of GHZ $(|\underline{00}\rangle + |\underline{11}\rangle)(|\underline{00}\rangle + |\underline{11}\rangle)$ to $(|\underline{00}\rangle + |\underline{11}\rangle)$. Other outcomes are equivalent to this up to a logical Pauli operation and translate to basis change in the final cluster-state qubit. The resulting state is a six-qubit GHZ state: $|000000\rangle + |111111\rangle$.

(II) Second, to further shrink this to a five-qubit GHZ state we measure one of the center spins in the basis of $|\pm\rangle \equiv (|0\rangle \pm |1\rangle)/\sqrt{2}$, and the resultant state for the remaining five qubits is $|00000\rangle + |11111\rangle$, up to a logical Pauli Z correction, which can be accounted for by a basis changed in later measurement procedure.

(III) Next we consider how to achieve the operation of CZ on two center qubits of two GHZ pairs. This again is done by measuring an associated bond particle (i.e., two virtual qubits) in a suitable basis. The four basis states are $CZ|\pm \pm\rangle$. It is equivalent to applying a CZ gate between the two virtual qubits, followed by a measurement in $\pm\pm$ basis. For illustration, we again denote the two GHZ pairs by $(|\underline{00}\rangle + |\underline{11}\rangle)(|\underline{00}\rangle + |\underline{11}\rangle)$. The CZ operation between the two virtual qubits transforms the state to $(|\underline{00}\rangle|\underline{00}\rangle + |\underline{00}\rangle|\underline{11}\rangle + |\underline{11}\rangle|\underline{00}\rangle - |\underline{11}\rangle|\underline{11}\rangle)$. Suppose $|+ +\rangle$ is obtained from measuring the two virtual qubits (i.e., the bond particle), the remaining spins are projected to $(|\underline{0}\rangle|\underline{0}\rangle + |\underline{0}\rangle|\underline{1}\rangle + |\underline{1}\rangle|\underline{0}\rangle - |\underline{1}\rangle|\underline{1}\rangle)$, i.e., a CZ gate has effectively applied between two center spins.

If all the bond particles are measured so as to induce CZ gates between neighboring center spins, as in (III), then the center spins will form a cluster state on the original honeycomb lattice at the end of the procedure. The consideration of faulty cluster state on the honeycomb lattice could be carried out as done in the case of the square lattice by Browne *et al.* [17] to extract the corresponding ratio $k(p_l)$. But doing this is beyond the scope of the present paper. Instead we use the result of $k(p_l)$ obtained in Ref. [17] for the faulty square-lattice cluster
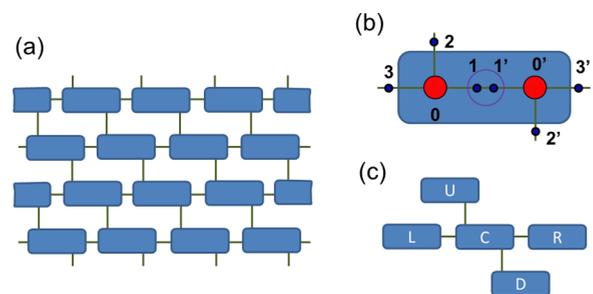

FIG. 6. (Color online) Generation of a cluster state on a square lattice: (a) original honeycomb (i.e., brick wall) lattice; (b) a block of spins that give rise to one logical cluster-state qubit; (c) a center logical block and its neighbor four blocks on a square lattice.

state to estimate the region where FTQC can be still be carried out. To do this, we should aim to convert our spin network to a cluster state on a square lattice. We note that although this may underestimate the region of universality our goal is to show the existence of such a region in both zero and nonzero temperatures.

To convert our original network of spins on the honeycomb lattice (see, e.g., Fig. 6) to form a cluster state on a square lattice, we group two units of spin blocks as shown in Fig. 3 to generate one logical qubit of a cluster state. We label the spins

as shown in Fig. 6(c). Virtual spins 1 and 1$'$ are used to merge two GHZ states. Center spin 0 will be removed so as to shrink the six-qubit GHZ to a five-qubit GHZ state. The remaining virtual qubits 2, 3, 2$'$, 3$'$ will combine with their partner virtual qubits to enact CZ gates on the center qubit 0$'$ with neighboring such center qubits. The result will be a cluster state on a square lattice. However, at finite temperatures thermal errors occur and the result is a faulty cluster state. We thus summarize the effect of (single-spin) errors on the logical qubits of the cluster state in Table II for reference.

[1] E. Fermi, *Thermodynamics* (Dover, New York, 2011).

[2] S. Sachdev, *Quantum Phase Transitions* (Cambridge University Press, Cambridge, England, 1999).

[3] M. Nielsen and I. Chuang, *Quantum Computation and Quantum Information* (Cambridge University Press, Cambridge, England, 2000).

[4] X.-G. Wen, *Quantum Field Theory of Many-Body Systems* (Oxford University Press, Oxford, 2004).

[5] D. Gottesman and I. L. Chuang, Nature (London) **402**, 390 (1999).

[6] M. A. Nielsen, Phys. Lett. A **308**, 96 (2003); D. W. Leung, Int. J. Quantum Inform. **02**, 33 (2004); A. M. Childs, D. W. Leung, and M. A. Nielsen, Phys. Rev. A **71**, 032318 (2005).

[7] R. Raussendorf and H. J. Briegel, Phys. Rev. Lett. **86**, 5188 (2001); R. Raussendorf, D. E. Browne, and H. J. Briegel, Phys. Rev. A **68**, 022312 (2003).

[8] H. J. Briegel, D. E. Browne, W. Dür, R. Raussendorf, and M. Van den Nest, Nat. Phys. **5**, 19 (2009).

[9] R. Raussendorf and T.-C. Wei, Annu. Rev. Condens. Matter Phys. **3**, 239 (2012).

[10] A. C. Doherty and S. D. Bartlett, Phys. Rev. Lett. **103**, 020506 (2009).

[11] A. Miyake, Phys. Rev. Lett. **105**, 040501 (2010).

[12] S. D. Bartlett, G. K. Brennen, A. Miyake, and J. M. Renes, Phys. Rev. Lett. **105**, 110502 (2010).

[13] D. V. Else, I. Schwarz, S. D. Bartlett, and A. C. Doherty, Phys. Rev. Lett. **108**, 240505 (2012).

[14] D. V. Else, S. D. Bartlett, and A. C. Doherty, New J. Phys. **14**, 113016 (2012).

[15] K. Fujii, Y. Nakata, M. Ohzeki, and M. Murao, Phys. Rev. Lett. **110**, 120502 (2013).

[16] D. Gross, J. Eisert, N. Schuch, and D. Perez-Garcia, Phys. Rev. A **76**, 052315 (2007).

[17] D. E. Browne, M. B. Elliott, S. T. Flammia, S. T. Merkel, A. Miyake, and A. J. Short, New. J. Phys. **10**, 023010 (2008).

[18] S. D. Barrett, S. D. Bartlett, A. C. Doherty, D. Jennings, and T. Rudolph, Phys. Rev. A **80**, 062328 (2009).

[19] A. S. Darmawan, G. K. Brennen, and S. D. Bartlett, New. J. Phys. **14**, 013023 (2012).

[20] Y. Li, D. E. Browne, L. C. Kwek, R. Raussendorf, and T.-C. Wei, Phys. Rev. Lett. **107**, 060501 (2011).

[21] F. Verstraete and J. I. Cirac, Phys. Rev. A **70**, 060302(R) (2004).

[22] T.-C. Wei, I. Affleck, and R. Raussendorf, Phys. Rev. Lett. **106**, 070501 (2011).

[23] A. Miyake, Ann. Phys. (Leipzig) **326**, 1656 (2011).

[24] J.-M. Cai, A. Miyake, W. Dür, and H. J. Briegel, Phys. Rev. A **82**, 052309 (2010).

[25] T.-C. Wei, R. Raussendorf, and L. C. Kwek, Phys. Rev. A **84**, 042333 (2011).

[26] K. Kieling, T. Rudolph, and J. Eisert, Phys. Rev. Lett. **99**, 130501 (2007).

[27] K. Fujii and T. Morimae, Phys. Rev. A **85**, 010304(R) (2012).

[28] R. Raußendorf, Int. J. Quantum Inform. **07**, 1053 (2009).

[29] A. M. Stephens, A. G. Fowler, and L. C. L. Hollenberg, Quantum Inf. Comput. **8**, 330 (2008).

[30] A. M. Stephens and Z. W. E. Evans, Phys. Rev. A **80**, 022313 (2009).

[31] R. Raussendorf, J. Harrington, and K. Goyal, Ann. Phys. **321**, 2242 (2006).

[32] Y. Li and S. C. Benjamin, New J. Phys. **14**, 093008 (2012).

[33] S. D. Barrett and T. M. Stace, Phys. Rev. Lett. **105**, 200502 (2010).